# Lyme disease and relapsing fever *Borrelia* elongate through zones of peptidoglycan synthesis that mark division sites of daughter cells

Brandon Lyon Jutras[a,b,c,1], Molly Scott[a,b,1], Bradley Parry[a,b], Jacob Biboy[d], Joe Gray[e], Waldemar Vollmer[d], and Christine Jacobs-Wagner[a,b,c,f,2]

[a]Microbial Sciences Institute, Yale University, West Haven, CT 06517; [b]Department of Molecular, Cellular, and Developmental Biology, Yale University, New Haven, CT 06516; [c]Howard Hughes Medical Institute, Yale University, New Haven, CT 06516; [d]Centre for Bacterial Cell Biology, Institute for Cell and Molecular Biosciences, Newcastle University, Newcastle upon Tyne NE2 4AX, United Kingdom; [e]Institute for Cell and Molecular Biosciences, Newcastle University, Newcastle upon Tyne NE2 4AX, United Kingdom; and [f]Department of Microbial Pathogenesis, Yale Medical School, New Haven, CT 06516

This contribution is part of the special series of Inaugural Articles by members of the National Academy of Sciences elected in 2015.

Contributed by Christine Jacobs-Wagner, July 5, 2016 (sent for review May 18, 2016; reviewed by Yves V. Brun and Scott Samuels)

**Agents that cause Lyme disease, relapsing fever, leptospirosis, and syphilis belong to the phylum Spirochaetae—a unique lineage of bacteria most known for their long, spiral morphology. Despite the relevance to human health, little is known about the most fundamental aspects of spirochete growth. Here, using quantitative microscopy to track peptidoglycan cell-wall synthesis, we found that the Lyme disease spirochete *Borrelia burgdorferi* displays a complex pattern of growth. *B. burgdorferi* elongates from discrete zones that are both spatially and temporally regulated. In addition, some peptidoglycan incorporation occurs along the cell body, with the notable exception of a large region at the poles. Newborn cells inherit a highly active zone of peptidoglycan synthesis at midcell that contributes to elongation for most of the cell cycle. Concomitant with the initiation of nucleoid separation and cell constriction, second and third zones of elongation are established at the 1/4 and 3/4 cellular positions, marking future sites of division for the subsequent generation. Positioning of elongation zones along the cell is robust to cell length variations and is relatively precise over long distances (>30 μm), suggesting that cells "sense" relative, as opposed to absolute, cell length to establish zones of peptidoglycan synthesis. The transition from one to three zones of peptidoglycan growth during the cell cycle is also observed in relapsing fever *Borrelia*. However, this mode of growth does not extend to representative species from other spirochetal genera, suggesting that this distinctive growth mode represents an evolutionary divide in the spirochete phylum.**

Lyme disease | *Borrelia burgdorferi* | peptidoglycan | relapsing fever | spirochetes

Lyme disease is a multisystem disorder that results in flu-like symptoms and, if left untreated, can develop into arthritis, carditis, and severe neurological complications. In recent years, the incidence and geographical range of Lyme disease have rapidly risen (1, 2), making it the most reported vector-borne disease in the United States. In North America, the primary causative agent of Lyme disease is the spirochetal bacterium *Borrelia burgdorferi* sensu stricto. Whereas most research efforts have focused on host invasion, immune response, and the gene regulatory mechanisms involved in pathogen transmission, comparatively little attention has been paid to the basic biology of this important pathogen (3). In particular, how this bacterium grows and divides remains unknown, despite the fact that these processes are essential for its proliferation. Our knowledge gap in the principles fundamental to cell growth and division extends to the entire spirochete phylum, which, besides *B. burgdorferi,* includes many important disease-causing agents, such as those responsible for syphilis, relapsing fever, and leptospirosis (4).

Spirochetes are unusual bacteria in many respects. For example, most spirochetes are very thin (~0.2 μm) and long (up to 150 μm) and have a spiral or undulated morphology. Despite similar morphological features, the phylum displays extensive niche diversity. Within the same family, some species live within the gut of termites or ticks, whereas close relatives are parasites or free-living saprophytes in marine environments. When laboratory-based propagation is possible, doubling times of spirochete cultures tend to be slow, and genetic manipulations are generally tedious. These challenges have undoubtedly contributed to a poor understanding of this intriguing group of bacteria.

In bacteria, cell growth and division are intimately linked to the expansion of the peptidoglycan (PG) cell wall. The PG meshwork, a gigadalton molecular sac that surrounds the cytoplasmic membrane, is composed of glycan strands cross-linked by short peptides containing D- and L-amino acids (5). In spherical bacteria, growth (i.e., formation of a new hemisphere in daughter cells) generally occurs through septal PG synthesis during the division process (6). Rod-shaped bacteria, however, must first elongate before septal synthesis and cell division can take place. Apart from a few reported exceptions (7), the elongation process typically involves the incorporation of new PG either along the cell cylinder (lateral growth) or from the cell poles (polar growth)

## Significance

**Spirochetes pose a significant threat to human and animal health, yet little is understood about how these bacteria grow and divide. We discovered that Lyme disease and relapsing fever spirochetes elongate by synthesizing peptidoglycan, a major component of the cell wall, in discrete zones that are spatially regulated over the cell cycle. Zones of cell growth are established in the previous generation and mark future sites of cell division in the next cell cycle. In contrast, other genera display nearly uniform cell wall synthesis, which is commonly reported in bacteria. The distinctive mode of growth exhibited by the Lyme disease and relapsing fever spirochetes may provide an avenue for the strategic design of targeted antimicrobial therapies.**

Author contributions: B.L.J., M.S., W.V., and C.J.-W. designed research; B.L.J., M.S., J.B., and J.G. performed research; B.L.J., M.S., B.P., J.G., W.V., and C.J.-W. analyzed data; and B.L.J., M.S., and C.J.-W. wrote the paper.

Reviewers: Y.V.B., Indiana University; and S.S., University of Montana.

The authors declare no conflict of interest.

See QnAs on page 9129.

[1]B.L.J. and M.S. contributed equally to this work.

[2]To whom correspondence should be addressed. Email: christine.jacobs-wagner@yale.edu.

This article contains supporting information online at www.pnas.org/lookup/suppl/doi:10.1073/pnas.1610805113/-/DCSupplemental.

(8). Elongation is then followed by septal PG synthesis and pole formation.

The recent development of chemical tools that probe PG synthesis (6, 9, 10) has transformed our ability to explore the morphogenesis of nonmodel bacteria (11, 12). In this study, we used fluorescent D-alanine analogs for cell imaging (6) and developed protocols for quantitative analysis to determine the growth pattern of several spirochetes. Our results revealed a striking split among spirochetal genera, with the *Borrelia* genus displaying a mode of bacterial growth in which sites of localized PG elongation predetermine the cell division site of the next generation.

## Results

Under our growth conditions (complete BSK II culture medium, 34 °C), the *B. burgdorferi* type strain B31 MI replicates every 8–12 h (Fig. S1*A*), over which time the bacterium elongates 23 ± 10 μm ($n$ = 276 cells, Fig. S1*B*). To get a snapshot of where new PG synthesis occurs, we incubated *B. burgdorferi* with the fluorescent D-alanine analog 7-hydroxycoumarin-amino-D-alanine (HADA) for 1 h. Fluorescent microscopy revealed a surprisingly complex pattern of HADA signal (Fig. 1*A*). Fluorescent signal was observed throughout most of the cell cylinder, suggestive of lateral PG synthesis, although many cells had extended regions corresponding to the cell poles that were largely devoid of signal (Fig. 1*B*, *Inset*). In some cells, one pole had HADA signal, but it likely reflects a remnant of the HADA incorporation that occurred at midcell during septal PG synthesis in the previous generation (Fig. S2*A*). However, the most striking feature of the HADA pattern was the presence of discrete zones of high signal (Fig. 1 *A* and *B*). We observed a similar pattern using the fluorescent D-alanine analog (R)-2-amino-3-((7-nitrobenzo[c][1,2,5]oxadiazol-4-yl)amino) propanoic acid hydrochloride (NADA) instead of HADA (Fig. S2*B*). Neither HADA nor NADA labeling had an impact on *B. burgdorferi* replication rate (Fig. S1*A*). We confirmed that the signal is from labeled PG, because purified PG sacculi displayed a fluorescent pattern with bright zones of accumulation and polar regions devoid of signal (Fig. 1 *C* and *D*), consistent with the live-cell observations (Fig. 1*B*). Furthermore, liquid chromatography–mass spectrometry (LC-MS) analysis of digested PG sacculi corroborated the mass shift expected for the addition of HADA into the fifth position of the pentapeptide, replacing the native terminal D-alanine (Fig. S3).

In principle, incorporation of the D-alanine analog HADA into PG can occur through periplasmic exchange (6) or through the cytoplasmic pool of PG precursors. The D-alanyl-D-alanine ligase, MurF, is required to produce the PG pentapeptides and is specifically inhibited by D-cycloserine (13). Cells coincubated with HADA and D-cycloserine displayed no signal above background (DMSO control), similar to cells treated with HADA and a 50-fold molar excess of unlabeled D-alanine (Fig. 1*E* and Fig. S2*C*). We concluded that HADA incorporates into the PG either via the cytoplasmic precursor pathway or via a periplasmic exchange reaction in the nascent PG catalyzed by penicillin-binding proteins (PBPs). Any of these possible incorporation mechanisms identifies sites of PG synthesis that occur during the time of HADA incubation.

We hypothesized that the complex spatial pattern of PG synthesis in *B. burgdorferi* might reflect the spatial arrangement of PBPs, which are periplasmic enzymes involved in the late stages of precursor incorporation into growing PG. To examine the localization of PBPs, we used bocillin, a fluorescent analog of penicillin (14). We first demonstrated that bocillin binds covalently to multiple PBPs in *B. burgdorferi* cell extracts and that this binding is specifically inhibited by the penicillin competitor cephalexin (Fig. S4 *A* and *B*). In live cells, bocillin signal seemed specific to PBPs (Fig. 2*A*) because it was abolished when cells were treated with cephalexin (Fig. S4 *C* and *D*). PBP

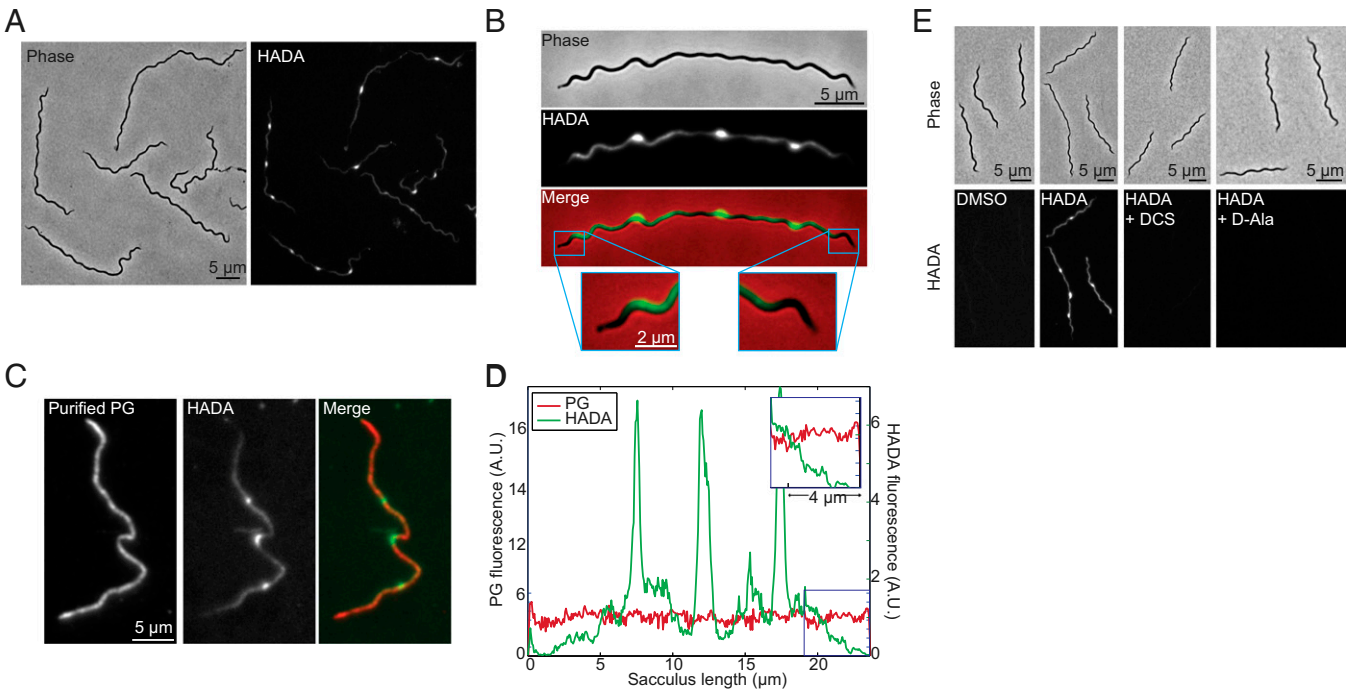


**Fig. 1.** Complex pattern of HADA incorporation into *B. burgdorferi* PG. (*A*) Phase-contrast and fluorescence micrographs of live *B. burgdorferi* B31 MI cells labeled with 0.1 mM HADA for 1 h. (*B*) Example of a HADA-labeled cell. (*C*) Fluorescence micrographs of a PG sacculus purified from HADA-labeled cells. The PG sacculus was identified by immunofluorescence staining with anti-PG antibodies (*Left*). (*D*) Fluorescence line scans of anti-PG antibody and HADA signals from the purified PG sacculus shown in *C*. (*E*) Micrographs of *B. burgdorferi* B31 MI cells incubated with 1% DMSO, 0.1 mM HADA alone (HADA), 0.1 mM HADA and 100 μg/mL MurE ligase inhibitor D-cycloserine (HADA + DCS), or 0.1 mM HADA and 5 mM D-alanine (HADA + D-Ala).

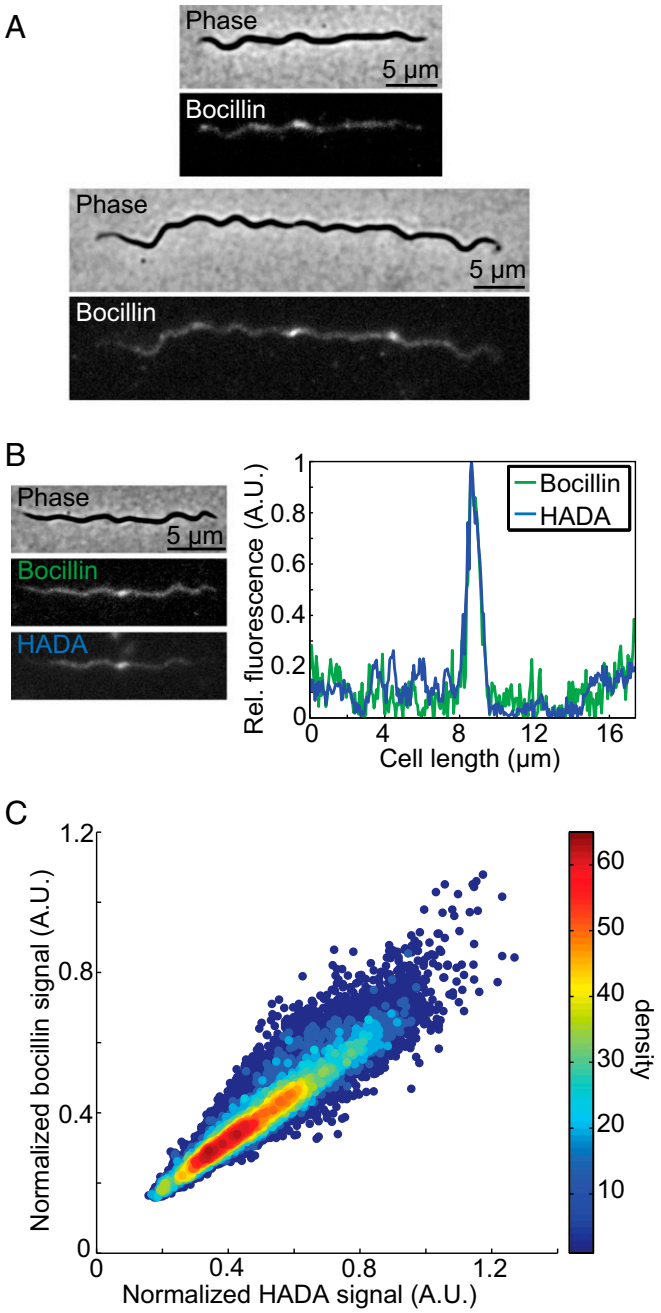


**Fig. 2.** Colocalization of HADA and fluorescent PBP analog bocillin. (*A*) Micrographs of *B. burgdorferi* B31 MI incubated for 30 min with 1.5 μg/mL of bocillin alone. (*B*) Representative micrograph and corresponding fluorescence profile of a cell colabeled with 1.5 μg/mL of bocillin and 40 μM of HADA. (*C*) Correlation analysis of HADA and bocillin signals. HADA and bocillin fluorescence intensities were normalized on a single-cell basis and compared ($n$ = 286 cells, $r$ = 0.96). The color map indicates density of plotted correlations.

localization displayed a pattern similar to that of HADA (Fig. 2*A*), as demonstrated by colabeling cells with concentrations of bocillin and HADA that did not result in signal bleed-through (Fig. 2*B* and Fig. S4 *E* and *F*). Colocalization was confirmed at the population level by correlation analysis of PBP and HADA fluorescent signal intensity, which yielded a strong positive correlation ($r$ = 0.96, Fig. 2*C*).

We noted that, in a population, the number of zones of active PG synthesis per cell seemed to increase with the size of the cell (Fig. 1*A*). Because cell length increases between cell birth and division, we wondered whether the spatial arrangement of HADA zones reflects a cell-cycle pattern. To examine this possibility, we constructed a demograph (15) in which the HADA profile was displayed for every cell, organized by increasing cell length. Using cell length as a proxy for cell-cycle progression revealed a striking pattern (Fig. 3*A*). Cells were born with a single HADA zone and retained this pattern for most of the cell cycle, after which secondary and tertiary HADA zones appeared (Fig. 3*A*). At the very end of the cell cycle (i.e., before cell separation), the primary zone disappeared (Fig. 3*A*). The zone positions and their spacing increased with cell length (Fig. 3*B*) such that, in terms of relative position, zones were spatially conserved at 1/4, 1/2, and 3/4 positions along the cell length (Fig. 3*C*). In the experiments showcased in Figs. 1 and 3, cells were labeled with HADA for 1 or 4 h, which corresponds to ∼10–40% of the cell cycle. Reducing the labeling time to 15 min (i.e., less than 5% of the cell cycle) produced similar results (Fig. S5), albeit with lower overall signal intensity.

These findings raised the question of whether zones of PG synthesis correspond to formation of septa. To assess this possibility, we performed photobleaching experiments using HADA-labeled cells that constitutively express free GFP in the cytoplasm. In short cells (i.e., at the beginning of the cell cycle), repeated laser pulses at a region away from the single midcell HADA zone resulted in photobleaching of GFP signal throughout the cell, indicating a contiguous cytoplasm and the absence of a septum at midcell (Fig. 4*A*). A septum eventually formed, but only late in the cell cycle, as shown in very long cells by the disappearance of GFP signal from only half of the cell body (Fig. 4*B*).

We noted that, before photobleaching, septation was visibly apparent by a depletion of GFP signal and phase-contrast intensity at midcell. We reasoned that signal intensity features could therefore be exploited to characterize the cell-cycle timing of 1/4 and 3/4 zone establishment. Cells constitutively expressing cytoplasmic GFP were labeled with HADA and stained with the DNA dye DRAQ5 (Fig. S6*A*). Signal intensity profiles were obtained from cell profile ensembles organized into groups based on similar signal features common in the GFP and DNA channels (*Materials and Methods*) and used here as a proxy for cell-cycle progression. We found that, during the time when the DNA and GFP signals were relatively smooth across the cell, the HADA signal displayed a single peak at midcell (Fig. 4*C*, stage i). The small "bump" seen in GFP signal near midcell may be due to a slight bleed-through from the HADA signal under the concentration of HADA used in this experiment. Importantly, the 1/4 and 3/4 zones became apparent just as the DRAQ5 and GFP signals started dipping at midcell (Fig. 4*C*, stage ii), indicating that establishment of these zones occurs at about the time when nucleoid separation and septation initiate. The 1/4 and 3/4 zones increased in intensity as DNA separation and septation proceeded (Fig. 4*C*, stages iii and iv), as indicated by the decrease in DRAQ5 and GFP fluorescence at midcell. A reduction in phase-contrast intensity at midcell became more apparent in late stages (Fig. 4*C*, stages iii and iv). The final cell-cycle stage when the HADA zone at midcell disappears was observed in few cells and therefore was not apparent in the ensemble profile. An example of this final cell-cycle stage is shown at the single-cell level (Fig. 4*C*, stage v).

*Borrelia* species face the unique pressure of torque exerted upon the cell cylinder by the axial periplasmic flagella that wrap around the PG layer (16). It has been suggested that the PG meshwork counteracts this constant stress (16, 17). The intense HADA signal at zones of PG synthesis might therefore represent localized areas where the cells have added multiple layers of PG to provide reinforcement to counteract flagella-mediated torque. Alternatively, the intense zones of PG synthesis may correspond to sites of PG elongation that contribute to cell length expansion. To evaluate whether the intense zones of HADA signal correspond

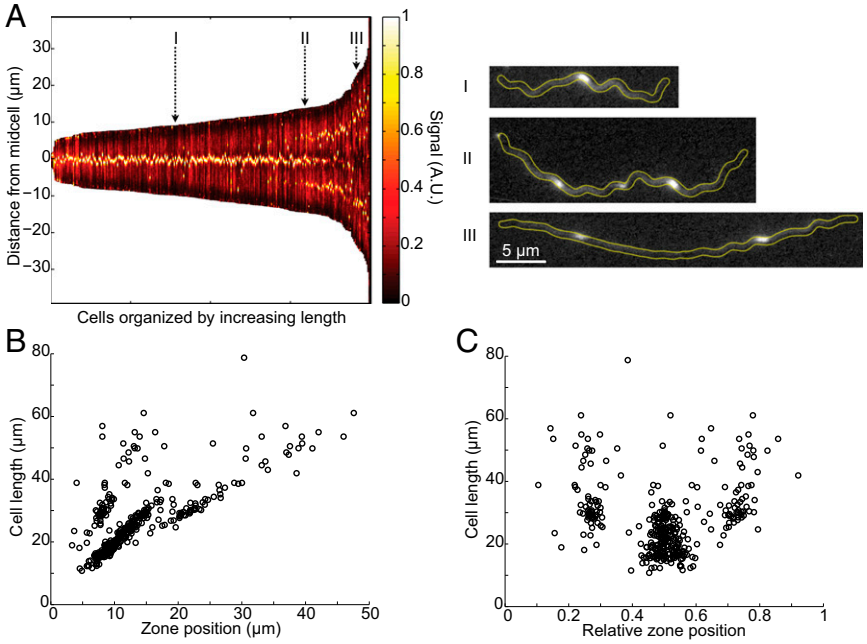


**Fig. 3.** Population analysis of HADA signal during the *B. burgdorferi* cell cycle. (*A*) Demograph analysis of HADA fluorescence profiles in which all B31 MI cells in the population ($n = 276$) were organized in ascending cell length order (left to right). The heat map displays the relative fluorescence in arbitrary units (0–1). Representative fluorescence images of cells (*I*, *II*, and *III*) at different points of the cell cycle (dashed arrows) are depicted on the right with cell boundaries in yellow. (*B*) Scatter plot showing the positions of HADA zone positions as a function of cell length. (*C*) Same as in *B*, except that zone positions were plotted in cellular coordinates.

to PG multilayering or elongation, we pulse-labeled *B. burgdorferi* for 1 h with NADA (green) and chased with HADA (red) for 1 h. If zones corresponded to an increase in PG layers, we would expect to see colocalization throughout the entire region, whereas if they were sites of cell elongation, the NADA signal (old PG synthesis) should be displaced by the HADA signal (new PG synthesis). The results were consistent with the latter, with old PG synthesis (NADA) flanking the site of new (HADA) synthesis (Fig. 4*D*). This indicates that the zones of PG synthesis contribute to PG expansion along the cell length. Note that we referred to these sites of localized cell elongation as "zones" as opposed to spots or foci because the size of the HADA signal, even after a labeling time as short as 15 min, was larger ($0.35 \pm 0.08$ μm, $n = 299$ cells) than that measured for diffraction-limited objects such as fluorescent beads ($0.11 \pm 0.015$ μm, $n = 1{,}014$) or GFP-μNS particles in *Escherichia coli* ($0.11 \pm 0.08$ μm, $n = 23{,}451$ cells) (Fig. S7*A*). This is also in contrast to the size of the HADA signal from septal synthesis in *E. coli*, which is closer to the diffraction limit ($0.27 \pm 0.06$ μm, $n = 86$) (Fig. S7).

*B. burgdorferi* sensu stricto is an umbrella term used to define all strains that are closely related to the type strain B31 MI (18). These strains exhibit genotypic variability (19, 20). Furthermore, under our laboratory conditions, we observed differences in cell length distribution among *B. burgdorferi* strains (Fig. S8*A*). Despite these differences, all strains displayed one zone of PG synthesis at midcell in short cells and three zones in longer cells, with the relative position of each zone abiding by the same 1/4, 1/2, and 3/4 rule (Fig. 5*A* and Fig. S8 *B*–*G*). The fraction of cells with one zone versus two or three zones differed between strains (Fig. 5*B*), suggesting a potential difference in the timing of secondary and tertiary zone formation. Temporal differences aside, cells from each strain established secondary and tertiary zones before cell separation, because virtually all cells from all strains examined had at least one zone (Fig. 5*B*), indicating that they were born with an active zone inherited from the previous generation. This growth pattern was also robust to cell length variations, because it was preserved in a flagellar Δ*flaB* mutant, which, on average, is much longer than wild type (21) (Fig. 5 and Fig. S8 *A* and *D*).

The genus *Borrelia* is not limited to Lyme disease pathogens but also includes spirochetes that cause relapsing fever. We found that the relapsing fever agents, *Borrelia hermsii* and *Borrelia miyamotoi*, displayed a pattern of PG synthesis similar to that of *B. burgdorferi* (Fig. 6 *A* and *B* and Fig. S9). The relative 1/4, 1/2, and 3/4 spacing was also conserved (Fig. S10), indicating that discrete zones of elongation are common among divergent *Borrelia* spp. Remarkably, we discovered that other spirochetes display a different mode of growth. For example, another member of the *Spirochaetaceae* family (4), the periodontal pathogen *Treponema denticola*, displayed dispersed growth along the cell length (Fig. 6*C* and Fig. S9*A*). A single zone of PG synthesis was apparent near midcell in long *T. denticola* cells (Fig. 6*C* and Fig. S9*A*), corresponding to septum formation at the end of the cell cycle. Treating cells with D-cycloserine prevented HADA incorporation (Fig. S9*B*), consistent with HADA labeling new PG incorporation. Similarly to *T. denticola*, the distantly related spirochete *Leptospira interrogans* (4, 22), which is responsible for the tropical disease leptospirosis, did not exhibit a *Borrelia*-like pattern of PG synthesis (Fig. 6*D* and Fig. S9*A*). Instead, the HADA signal was mostly dispersed, although some cells showed higher signal across a broad region at midcell (Fig. 6*D* and Fig. S9*A*). Only in long *L. interrogans* cells was a single zone of HADA accumulation present (Fig. 6*D* and Fig. S9*A*), reflecting septal PG synthesis. Importantly, none of the non-*Borrelia* spirochetes were born with a single HADA zone at midcell or formed secondary zones at 1/4 and 3/4 positions (Fig. 6 *C*–*E*), indicating that this mode of growth is a distinctive feature of *Borrelia*.

## Discussion

This study represents an effort to understand how spirochetes, a biologically and evolutionarily unique group of bacteria, grow. Using PG synthesis as a tracer for cell growth, we uncovered an

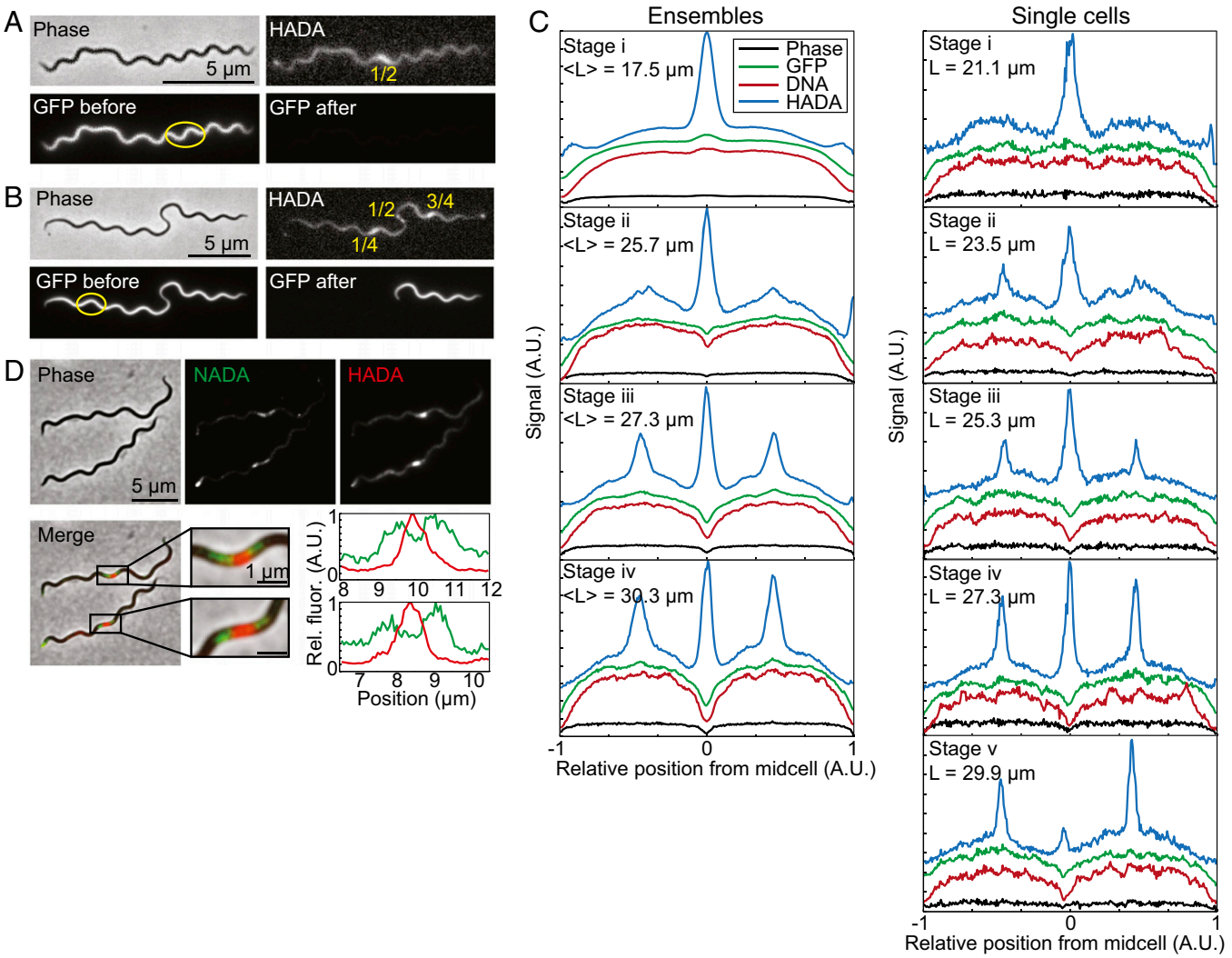


**Fig. 4.** Zones of PG synthesis are sites of elongation that mark future division sites. (*A*) *B. burgdorferi* Bb914 cells, which constitutively express GFP, were incubated for 4 h with 0.1 mM HADA and imaged before and after repeated laser photobleaching. A relatively short (21.7-μm) cell with a single HADA zone at midcell (early cell-cycle stage) is shown. The yellow oval shows the photobleaching region. (*B*) Same as in *A*, but showing a comparatively longer (33.9-μm) cell with 1/4 and 3/4 HADA zones, in addition to a fading midcell zone (late stage of cell cycle). (*C*) Ensemble (*Left*) and single-cell (*Right*) profiles of free cytoplasmic GFP (green), DRAQ5 DNA stain (red), HADA (blue), and phase-contrast (black) for *B. burgdorferi* strain Bb914 cells were plotted relative to midcell to track progression of cytoplasmic membrane fusion, nucleoid separation, and cell envelope separation relative to PG zone establishment. Fluorescence and phase-contrast intensities were normalized and plotted in arbitrary units (A.U.). Mean cell length (<L>) for each ensemble was displayed for ensemble profiles, and length (L) was displayed for single-cell profiles. Only cell bins displaying major cell-cycle events are shown. All profile ensembles are shown in Fig. S6*B*. (*D*) *B. burgdorferi* B31 MI cells were pulse-labeled for 1 h with 0.2 mM NADA (green) then chased with 0.1 mM HADA (red) for 1 h before imaging. Fluorescence profiles of zoomed regions depict the amount of overlap between signals.

unusual pattern of bacterial growth that changes during the cell cycle (Fig. S11). In *B. burgdorferi*, some PG synthesis occurs throughout most of the cell cylinder, except the cell poles (Fig. 1). Inert poles are a common trait among bacteria that elongate through lateral PG synthesis (23, 24); however, in these instances, only the polar caps seem inert. In the case of *B. burgdorferi*, the lack of HADA signal in purified PG extends well beyond the polar ends, ranging in the micrometer scale (Fig. 1*D*, *Inset*). Another surprising feature of the *B. burgdorferi* growth pattern is the presence of active zones of elongation that are temporally and spatially regulated (Fig. 3). Cells are born with a zone of active PG elongation at the middle of the cell. This zone, which is established in the previous generation, remains active throughout most of the cell cycle until secondary and tertiary zones are established at 1/4 and 3/4 positions at about the time the nucleoid starts segregating (Fig. 4*C* and Fig. S11). Initiation of nucleoid segregation also seems associated with the beginning of septal PG synthesis and cell constriction (Fig. 4*C* and Fig. S11). Interestingly, although there is cell-to-cell variability, it seems that, on average, the establishment of the 1/4 and 3/4 zones in *B. burgdorferi* occurs before DNA segregation and the septum are completed (Fig. 4*C* and Fig. S11). This suggests that cells are able to "sense" the cellular 1/4 and 3/4 positions to establish zones of PG synthesis.

*B. burgdorferi* is, in some aspects, similar to the firmicute *Streptococcus pneumoniae*, because *S. pneumoniae* is born with a ring of PG synthesis at midcell and establishes new rings of PG synthesis at 1/4 and 3/4 positions before division and cell separation are complete (25, 26). However, there are important differences between *B. burgdorferi* and *S. pneumoniae*. In *B. burgdorferi*, unlike in *S. pneumoniae*, the intense zones of growth are wide (beyond the diffraction limit) and PG synthesis also occurs throughout the cell body with the notable exception

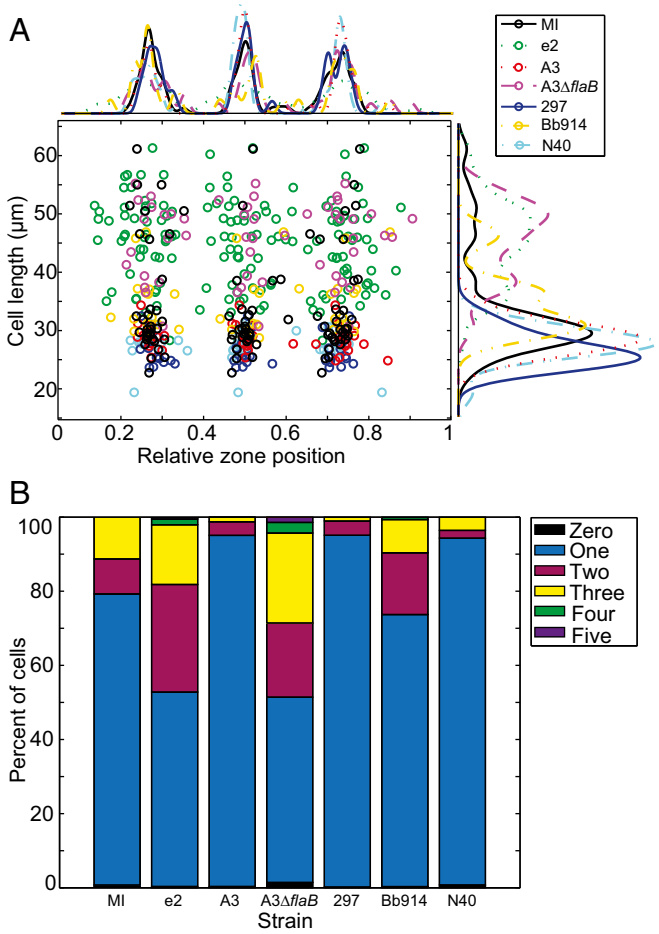


**Fig. 5.** Strains of *B. burgdorferi* exhibit a similar pattern of PG synthesis. (*A*) Scatter plot of the relative position of HADA zones as a function of cell length for various strains of *B. burgdorferi*. Only cells with three zones are plotted. Analysis was performed on B31 MI ($n = 33$), variant clones e2 ($n = 95$) and A3 ($n = 21$), and an A3 mutant lacking flagellar gene *flaB* (A3Δ*flaB*, $n = 18$). B31 derivatives were compared with clones of the human isolate 297 ($n = 20$) and tick isolate N40 ($n = 24$), as well as the strain Bb914 ($n = 30$). Probability distributions of plotted data are also shown. (*B*) Bar graphs depicting the percent of cells with a given number of zones.

of an extended region of the cell poles. Perhaps more importantly, the spatial and temporal regulation of PG synthesis contributing to either cell elongation or septum formation are vastly different between *B. burgdorferi* and *S. pneumoniae*, ultimately shaping their cell morphology. In *S. pneumoniae*, cell elongation occurs at the same time and place as septum formation, such that cells adopt a prolate spheroid shape (6, 25–29). This is in contrast to *B. burgdorferi*, in which cell elongation and septum formation are largely uncoupled, resulting in long, rod-shaped cells. This highlights the diversity in bacterial cell biology as well as the importance of expanding studies beyond the traditionally studied phyla.

The molecular mechanisms underlying the *Borrelia* mode of elongation remain to be elucidated. Because zones of cell elongation mark future sites of cell division (Fig. 4), one potential candidate for directing PG synthesis at elongation zones through PBP recruitment is the cell division protein FtsZ. In the proteobacterium *Caulobacter crescentus* (30), and to a lesser degree in *E. coli* (23, 31), cell elongation is bimodal, because lateral growth is followed by "preseptal" elongation in which FtsZ directs PG incorporation along the cell length before initiating septal PG synthesis. Perhaps, in the case of *Borrelia*, secondary and tertiary FtsZ rings form such that each daughter cell inherits an established FtsZ ring. Although FtsZ is a good candidate for directing PG elongation in *B. burgdorferi*, it is likely to be more complicated because the relatively large size of short-pulse-labeled HADA zones (Fig. S7) suggests that sites of elongation are substantially wider than what might be expected for a (static) FtsZ ring.

Although temporal differences may exist between commonly used laboratory *B. burgdorferi* strains, the overall growth pattern was maintained despite variability in cell length (Fig. 5). Even in the case of a flagellar mutant, which is much longer than wild-type *B. burgdorferi* and lacks its characteristic serpentine morphology (21) (Fig. 5 and Fig. S8*A*), PG synthesis at the relative 1/4, ½, and 3/4 positions was preserved (Fig. 5 and Fig. S8*D*). This implies that *B. burgdorferi* is able to regulate its growth pattern over long (>30 μm) and variable distances by "sensing" its relative, rather than absolute, length.

The divergence of spirochetes from other bacteria is thought to have occurred during early evolutionary history. Our study shows a striking divide in modes of growth within the spirochete phylum—members of the *Treponema* and *Leptospira* genera primarily elongate via a dispersed/lateral mode of growth, whereas species of the *Borrelia* genus display a zone-based pattern that is spatially and temporally regulated (Fig. 6). With the recent explosion in whole-genome sequence data, phylogenetic relationships are being reevaluated. Recent analysis has questioned the monophyletic nature of the spirochete phylum, proposing that *Borrelia* represents a unique clade that arose from a common ancestor that is distinct from the remaining genera in the *Spirochaetaceae* family (22). From a growth mode perspective, our results support this division (Fig. 6) and suggest a close evolutionary relationship between the divergent Lyme disease and relapsing fever clades.

The mode of cell growth in *Borrelia* also showcases spatial organization in these bacteria. It will be important to examine in the future whether other essential processes are spatially regulated inside the cells. For example, *Borrelia* may rely on spatial organization to maintain their highly segmented genome. These spirochetes differ from other members of the phylum and even the bacterial kingdom by having over 20 genetic elements, including many linear episomes (18, 32, 33). Whether the replication and segregation of these elements relate to the mode of growth of these cells and depend on spatial mechanisms remains to be explored.

As an essential biopolymer specific to bacteria, PG plays a major role in antibacterial susceptibility and resistance, in addition to being a major determinant in innate immune surveillance. With the exception of doxycycline, recommended treatment options for Lyme disease target PG synthesis (34), but in a nondiscriminatory manner. Broad-spectrum antibiotics of this nature have significant effects on the normal microbiota. The unique mode of growth described here may provide an opportunity for the development of therapeutic interventions tailored specifically to the PG synthesis of the Lyme disease and relapsing fever spirochetes.

## Materials and Methods

**Bacterial Strains and Culture Conditions.** Unless specifically noted, all experiments were performed on a clone of the type strain B31 MI (18). Clones of the human and tick isolates, 297 and N40, respectively, have been previously described (35, 36). A3, an infectious derivative of B31 MI, and the A3 clone lacking the *flaB* gene have been described elsewhere (21, 37). The high passage variant of B31 MI, B31 clone e2, was generated and characterized previously (38). Bb914, a derivative of 297 that expresses cytoplasmic GFP from the stable episome cp26, has been described previously (39).

Before analysis, all *B. burgdorferi* and *Borrelia hermsii* strains were propagated at 34 °C in BSK II culture medium supplemented with 6% (vol/vol) rabbit serum until the culture reached midlog exponential phase (40, 41). *B. miyamotoi* LB-2001 was cultured at 34 °C in the recently described medium MKP-F (42). *L. interrogans* serovar Copenhageni strain Fiocruz L1-130 (43) was expanded at 30 °C with gentle agitation in EMJH complete medium (44). *T. denticola* ATCC 34505 was propagated at 37 °C in supplemented TYGVS medium (45) in an anaerobic chamber under an atmosphere mixture of $N_2$:$H_2$:$CO_2$ (80:10:10).

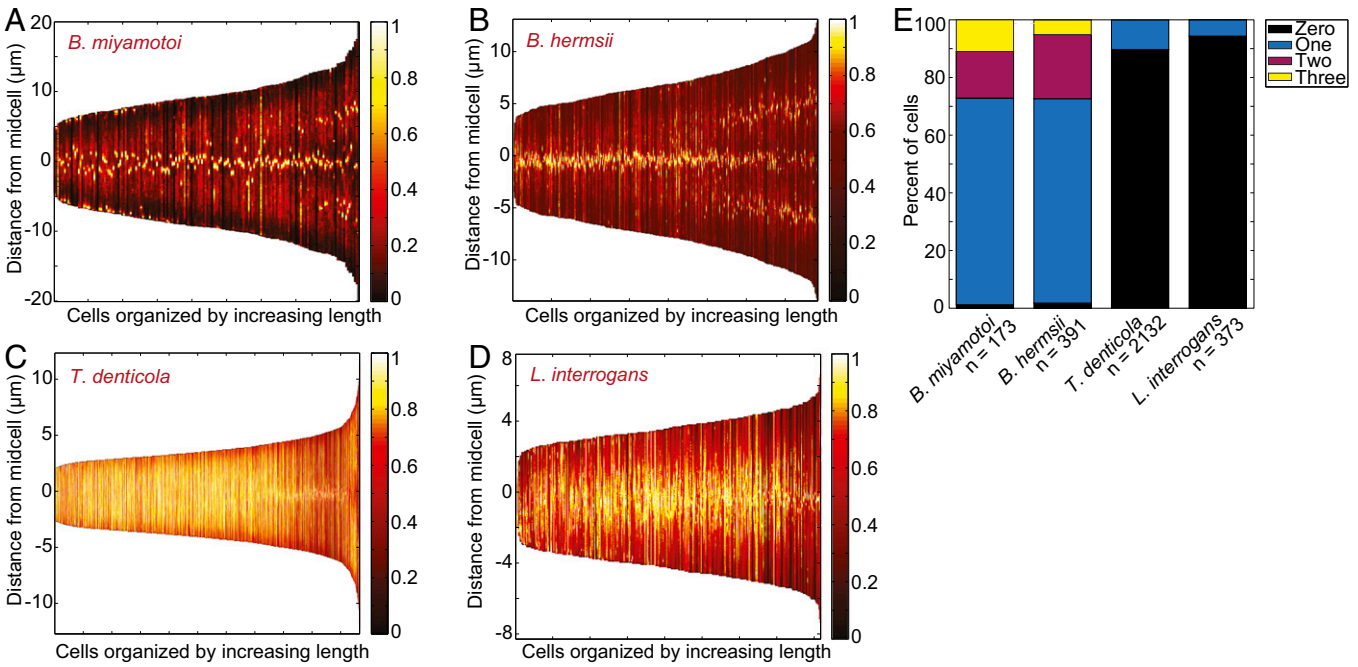


**Fig. 6.** A phylogenetic split in spirochete mode of growth. (*A–D*) Cultures of spirochetes from different genera were incubated with variable concentrations of HADA for 30 min and analyzed at the single-cell level in a demograph. Heat map displays the relative fluorescence intensity in arbitrary units (0–1). (*A*) *Borrelia miyamotoi* strain LS-2000, 0.1 mM HADA, $n = 173$. (*B*) *B. hermsii*, 0.1 mM HADA, $n = 391$. (*C*) *T. denticola* ATCC 34505, 0.2 mM HADA, $n = 2132$. (*D*) *L. interrogans* serovar Conpenhageni strain Fiocruz L1-130, 0.4 mM HADA, $n = 373$. (*E*) Bar graphs depicting the percent of cells with a given number of zones.

**In Vitro Identification of PBPs.** *B. burgdorferi* B31 MI (100 mL) was cultured to midlog exponential growth, harvested, and washed with, and resuspended in, PBS. Cells were lysed by sonication. Lysates were centrifuged at low speed (500 × *g* for 5 min) to remove unlysed cells. Membrane fractions were collected following ultracentrifugation at 110,000 × *g* for 30 min and resuspended in PBS supplemented with 100 mM NaCl. Equal amounts of membrane fraction volumes were mixed with 10 μg/mL bocillin (ThermoFisher Scientific) or 10 μg/mL bocillin with increasing amounts of cephalexin as indicated. Mixtures were incubated at 30 °C for 30 min before separating bound species by SDS/PAGE. Bocillin-labeled *B. burgdorferi* PBPs were visualized using a GE Typhoon 900.

**HADA and NADA Synthesis.** Both HADA and NADA were synthesized by the Yale Center for Molecular Discovery. HADA was synthesized as previously described (46), whereas NADA was synthesized using an alternative method (*Chemical Synthesis of NADA* and Fig. S12) that both reduced the number of steps and increased product yield.

**PG Purification and MS Analysis.** For the purification of PG sacculi, we adapted a protocol originally designed for *E. coli* (47). Specifically, a 450-mL culture of *B. burgdorferi* B31 MI was incubated with 0.1 mM HADA and 1% DMSO (final concentration) for 4 h. Labeled cells were harvested by centrifugation at 3,000 × *g* and washed twice with PBS. Cell suspensions were added dropwise to 8% (wt/vol) of boiling SDS, which created a final SDS concentration of 4%. Lysates were boiled for 1 h and PG sacculi were harvested by ultracentrifugation at 100,000 × *g* for 30 min at 32 °C. Contaminating SDS was removed by excessively washing PG sacculi with water before protein digestion with 0.5 mg/mL α-chymotrypsin in 1 mM $CaCl_2$ and 2 mM HCl. Proteases were denatured by boiling in 1% SDS for 30 min and purified PG sacculi were harvested by ultracentrifugation as described above and washed eight times with 10 mL of ultrapure water to remove contaminants and any possible carryover of SDS. Purified, HADA-labeled PG sacculi and control samples (with DMSO instead of HADA) were digested with cellosyl and the resulting muropeptides were analyzed by LC-MS as reported previously (48).

**PBP, DNA, and PG Labeling.** All HADA and NADA labeling experiments of live spirochetes included a final concentration of 1% DMSO (diluent). Incubation times (15 min to 4 h) and concentrations (0.04–0.4 mM) varied depending on the bacterial species and the specific experiment, as noted in the text. The concentrations of HADA and NADA used for each species were optimized based on the following criteria: (*i*) acceptable signal/background noise ratio as determined by evaluating fluorescence micrographs, (*ii*), solubility of HADA in each culture medium, and (*iii*) lack of adverse effect on bacterial replication rate (Figs. S1*A* and S13). Live-cell PBP labeling, with and without HADA, occurred for 30 min with 1.5 μg/mL of bocillin or diluent control (PBS). *B. burgdorferi* DNA staining occurred after HADA labeling with 0.5 μM DRAQ5. Following all labeling experiments, cells were gently harvested by centrifugation and washed twice with, and resuspended in, PBS.

For detection of PG by immunofluorescence microscopy, PG sacculi were purified as described above. Following purification, aliquots of HADA-labeled and DMSO control PG preparations were spotted on poly-lysine-coated slides and blocked with 3% (wt/vol) BSA in PBS supplemented with 0.05% Tween 20 (PBS-T) for 30 min. Affinity-purified antiserum against *E. coli* PG (anti-murein antibody) was a gift from Heinz Schwartz, Max-Planck Institute for Developmental Biology, Tuebingen, Germany, and Miguel de Pedro, Centro de Biología Molecular (CBM) Severo Ochoa, Consejo Superior de Investigaciones Científicas (CSIC)-Universidad Autónoma de Madrid (UAM), Madrid. Anti-murein antibody [1:10 in 1.5% (wt/vol) BSA/PBS-T] or diluent control were incubated with PG sacculus preparations for 1 h, washed with PBS-T, and incubated with goat anti-rabbit IgG conjugated to rhodamine (Jackson ImmunoResearch) [1:200 in 1.5% (wt/vol) BSA/PBS-T] for 1 h. After additional washing, samples were visualized as described below.

**Microscopy and Image Acquisition.** Most samples were spotted on 2% (wt/vol) agarose/PBS pads and imaged at room temperature. Imaging of purified PG sacculi and *L. interrogans* cells was facilitated by immobilization on poly-lysine-coated slides; the latter was necessary for *Leptospira* cells due to the focal plane issues caused by the highly coiled nature of these cells. Epifluorescence microscopy was performed on an Eclipse TiE microscope (Nikon) equipped with sCMOS camera (Andor) or Orca-R2 camera (Hamamatsu) and an oil-immersion phase-contrast objective Plan Apochromat 100×/1.45 N.A. (Nikon). Typical exposure times for phase-contrast image acquisition were 50–100 ms, whereas exposure times for epifluorescence imaging varied from 50 ms to 2 s.

**Photobleaching Experiments.** Photobleaching experiments were performed on Bb914 cells (39) labeled with 0.1 mM HADA for 4 h. Cells were imaged using a Nikon E80i microscope with an Andor iXonEM+ DU-897 camera. Cells were photobleached using a Photonic Instrument Micropoint laser system (CITY) at the wavelength 488 nm. Laser was pulsed at 10–12 discrete points in a region of the cell for 80–100 pulses (~30 s) to ensure complete bleaching of freely diffusing GFP with minimal damage to the cell.

**Postprocessing and Quantitative Analysis.** Postimage processing was performed by microscopy software MetaMorph and Nikon Elements. Any direct fluorescent intensity comparisons were made using the same look-up table values and applying these values to each experimental condition. Quantitative microscopy analysis was facilitated by the recently described software package Oufti (49). All subsequent analysis was performed using custom-made MATLAB scripts, which have been collated and supplied in Datasets S1–S18. Zones of PG synthesis were determined by finding peaks in fluorescence signal that were verified on a single-cell level (peakFinder_cellCheck.m). Zones occurring at the poles of cells (<5% of cell length from cell's end) were ultimately excluded from analysis. Signal correlation was performed by setting the sum of an Oufti-measured signal to 1 and normalizing by the area of cell mesh segments. MATLAB's built-in function corrcoef was used to calculate correlation coefficients.

**Point Spread Function Determination.** TetraspeckTM Microspheres (ThermoFisher; hereafter referred to as beads) were imaged through stacks of focal planes at 0.1-μm intervals. Using a custom-built script (findSigma.m), fluorescent beads were tracked through the stack and each fluorescence spot was fit to a Gaussian. From this Gaussian fit, the sigma of each fit was extracted. The theoretical point spread function (PSF) of the microscope was determined to be the average of the minimum sigma for each bead tracked through the different focal planes.

**Width of HADA Signal.** Fluorescent signal from *B. burgdorferi* B31 MI cells labeled for 15 min with HADA was compared with signal from 0.1-μm beads, signal from the diffraction-limited GFP-μNS particles in *E. coli* cells, as well as signal from HADA incorporation at the division site in *E. coli* MG1655 cells labeled for 3 min with 1 mM HADA in M9 medium supplemented with 1% glucose and 0.1% casamino acids.

After cell detection using Oufti, signal fluorescence information was output to MATLAB for analysis. Assuming that a one-dimensional fluorescence profile is uniformly distributed with length $w$, and that each point light source has a characteristic PSF around its source, $x$, the profile of the distributed fluorescence can be assumed as the integral convolution of the PSF and the actual fluorescence distribution, or

$$I(x) = \int_{-\infty}^{\infty} C(x_0)\mathrm{PSF}(x - x_0)dx_0,$$

assuming that $C(x_0)$ has square profiles

$$C(x_0) = H(x_0) - H(x_0 + w),$$

where $H(x)$ are Heaviside (step) functions and $w$ is the width of $C(x_0)$.

If we approximate the PSF as a Gaussian, we can solve for the final fitting function:

$$I(x) = \frac{1}{\sqrt{2}}\left(\mathrm{erf}\left(\frac{x}{\sqrt{2}\sigma}\right) - \mathrm{erf}\left(\frac{x}{\sqrt{2}\sigma} - w\right)\right).$$

Using this fitting function, we used MATLAB scripts (calculate_widths.m and fitErf.m) to determine the width, $w$, of the fit to each zone of high fluorescence. For the *E. coli* cells, to determine the width of the peak in fluorescence signal at the division site, cells were first thresholded by size to select only cells at late cell-cycle stages. We then screened long cells to verify that peaks were present at the division site with a minimum fluorescence threshold.

**Ensemble Profile Construction.** A surface specified by the degree of constriction in Oufti generated GFP and DRAQ5 (DNA) signals was used to weight a cell's inclusion in any given ensemble profile. Center points $X$, $Y$ for ensemble profiles were chosen on this surface as points along a ridge of local density maxima. The similarity of each cell to any given ensemble center was measured as the $L^2$ distance of that cell's degree of constriction in GFP and DNA signals to a given ensemble center. Weights, $W$, were obtained for each cell in each ensemble centered on $X$ and $Y$ as

$$W = \frac{1}{2\pi\sigma^2} e^{-\frac{(\mathrm{GFP}-X)^2 + (\mathrm{DNA}-Y)^2}{2\sigma^2}}.$$

A cell's fluorescent profiles were weighted to an ensemble if

$$W > \frac{1}{2\pi\sigma^2} \Big/ 2.$$

**Miscellaneous Scripts.** All MATLAB scripts and a full description of their functions can be found in Datasets S1–S18 and *MATLAB Scripts*, respectively.

**ACKNOWLEDGMENTS.** We thank Drs. Brian Stevenson, Erol Fikrig, Joppe Jovius, Alex Wagemarkers, Alan Barbour, Chris Fenno, Elsio Wunder, and Albert Ko for providing bacterial strains; Drs. Yves Brun and Michael VanNieuwenhze for generously providing us with aliquots of fluorescent D-amino acids that were instrumental to begin this project; and Drs. Andrew Goodman and Whitman B. Schofield for assistance with, and use of, their anaerobic chamber. We also thank members of the C.J.-W. laboratory for valuable discussion and critical reading of the manuscript. Work in W.V.'s laboratory was funded by Wellcome Trust Grant 101824/Z/13/Z. C.J.-W. is an Investigator of the Howard Hughes Medical Institute. This work was supported in part by National Institutes of Health Grant T32 GM007499, a Gruber Science Fellowship, and an M. Lelyn Branin Fellowship (all to M.S.).

1. Centers for Disease Control and Prevention (2013) CDC provides estimate of Americans diagnosed with Lyme disease each year. Available at www.cdc.gov/media/releases/2013/p0819-lyme-disease.html. Accessed February 17, 2016.
2. Mead PS (2015) Epidemiology of Lyme disease. *Infect Dis Clin North Am* 29(2):187–210.
3. Benach JL, et al. (2010) *Borrelia: Molecular Biology, Host Interaction and Pathogenesis*, eds Samuels DS, Radolf JD (Caister Academic, Norfolk, UK), pp 7–442.
4. Paster BJ, et al. (1991) Phylogenetic analysis of the spirochetes. *J Bacteriol* 173(19):6101–6109.
5. Vollmer W, Blanot D, de Pedro MA (2008) Peptidoglycan structure and architecture. *FEMS Microbiol Rev* 32(2):149–167.
6. Kuru E, et al. (2012) *In situ* probing of newly synthesized peptidoglycan in live bacteria with fluorescent D-amino acids. *Angew Chem Int Ed Engl* 51(50):12519–12523.
7. Randich AM, Brun YV (2015) Molecular mechanisms for the evolution of bacterial morphologies and growth modes. *Front Microbiol* 6:580.
8. Flärdh K, Buttner MJ (2009) Streptomyces morphogenetics: Dissecting differentiation in a filamentous bacterium. *Nat Rev Microbiol* 7(1):36–49.
9. Lebar MD, et al. (2014) Reconstitution of peptidoglycan cross-linking leads to improved fluorescent probes of cell wall synthesis. *J Am Chem Soc* 136(31):10874–10877.
10. Shieh P, Siegrist MS, Cullen AJ, Bertozzi CR (2014) Imaging bacterial peptidoglycan with near-infrared fluorogenic azide probes. *Proc Natl Acad Sci USA* 111(15):5456–5461.
11. Jiang C, Brown PJ, Ducret A, Brun YV (2014) Sequential evolution of bacterial morphology by co-option of a developmental regulator. *Nature* 506(7489):489–493.
12. Liechti GW, et al. (2014) A new metabolic cell-wall labelling method reveals peptidoglycan in *Chlamydia trachomatis*. *Nature* 506(7489):507–510.
13. Strominger JL, Eiji I, Threnn RH (1960) Competitive inhibition of enzymatic reactions by oxamycin. *J Am Chem Soc* 82(4):998–999.
14. Zhao G, Meier TI, Kahl SD, Gee KR, Blaszczak LC (1999) BOCILLIN FL, a sensitive and commercially available reagent for detection of penicillin-binding proteins. *Antimicrob Agents Chemother* 43(5):1124–1128.
15. Hocking J, et al. (2012) Osmolality-dependent relocation of penicillin-binding protein PBP2 to the division site in *Caulobacter crescentus*. *J Bacteriol* 194(12):3116–3127.
16. Yang J, Huber G, Wolgemuth CW (2011) Forces and torques on rotating spirochete flagella. *Phys Rev Lett* 107(26):268101.
17. Dombrowski C, et al. (2009) The elastic basis for the shape of *Borrelia burgdorferi*. *Biophys J* 96(11):4409–4417.
18. Fraser CM, et al. (1997) Genomic sequence of a Lyme disease spirochaete, *Borrelia burgdorferi*. *Nature* 390(6660):580–586.
19. Brisson D, Drecktrah D, Eggers CH, Samuels DS (2012) Genetics of *Borrelia burgdorferi*. *Annu Rev Genet* 46:515–536.
20. Casjens SR, et al. (2012) Genome stability of Lyme disease spirochetes: Comparative genomics of *Borrelia burgdorferi* plasmids. *PLoS One* 7(3):e33280.
21. Motaleb MA, et al. (2000) *Borrelia burgdorferi* periplasmic flagella have both skeletal and motility functions. *Proc Natl Acad Sci USA* 97(20):10899–10904.
22. Gupta RS, Mahmood S, Adeolu M (2013) A phylogenomic and molecular signature based approach for characterization of the phylum Spirochaetes and its major clades: Proposal for a taxonomic revision of the phylum. *Front Microbiol* 4:217–229.
23. de Pedro MA, Quintela JC, Höltje JV, Schwarz H (1997) Murein segregation in *Escherichia coli*. *J Bacteriol* 179(9):2823–2834.
24. Mobley HL, Koch AL, Doyle RJ, Streips UN (1984) Insertion and fate of the cell wall in *Bacillus subtilis*. *J Bacteriol* 158(1):169–179.
25. Peters K, et al. (2014) *Streptococcus pneumoniae* PBP2x mid-cell localization requires the C-terminal PASTA domains and is essential for cell shape maintenance. *Mol Microbiol* 92(4):733–755.
26. Tsui HC, et al. (2014) Pbp2x localizes separately from Pbp2b and other peptidoglycan synthesis proteins during later stages of cell division of *Streptococcus pneumoniae* D39. *Mol Microbiol* 94(1):21–40.
27. Morlot C, Noirclerc-Savoye M, Zapun A, Dideberg O, Vernet T (2004) The D,D-carboxypeptidase PBP3 organizes the division process of *Streptococcus pneumoniae*. *Mol Microbiol* 51(6):1641–1648.
28. Pinho MG, Kjos M, Veening JW (2013) How to get (a)round: Mechanisms controlling growth and division of coccoid bacteria. *Nat Rev Microbiol* 11(9):601–614.
29. Massidda O, Nováková L, Vollmer W (2013) From models to pathogens: How much have we learned about *Streptococcus pneumoniae* cell division? *Environ Microbiol* 15(12):3133–3157.
30. Aaron M, et al. (2007) The tubulin homologue FtsZ contributes to cell elongation by guiding cell wall precursor synthesis in *Caulobacter crescentus*. *Mol Microbiol* 64(4):938–952.

31. Varma A, de Pedro MA, Young KD (2007) FtsZ directs a second mode of peptidoglycan synthesis in *Escherichia coli*. *J Bacteriol* 189(15):5692–5704.
32. Barbour AG, Garon CF (1987) Linear plasmids of the bacterium *Borrelia burgdorferi* have covalently closed ends. *Science* 237(4813):409–411.
33. Ferdows MS, Barbour AG (1989) Megabase-sized linear DNA in the bacterium *Borrelia burgdorferi*, the Lyme disease agent. *Proc Natl Acad Sci USA* 86(15):5969–5973.
34. Wormser GP, et al. (2006) The clinical assessment, treatment, and prevention of Lyme disease, human granulocytic anaplasmosis, and babesiosis: Clinical practice guidelines by the Infectious Diseases Society of America. *Clin Infect Dis* 43(9): 1089–1134.
35. Steere AC, et al. (1984) Recovery of Lyme disease spirochetes from patients. *Yale J Biol Med* 57(4):557–560.
36. Barthold SW, Moody KD, Terwilliger GA, Jacoby RO, Steere AC (1988) An animal model for Lyme arthritis. *Ann N Y Acad Sci* 539:264–273.
37. Elias AF, et al. (2002) Clonal polymorphism of *Borrelia burgdorferi* strain B31 MI: Implications for mutagenesis in an infectious strain background. *Infect Immun* 70(4): 2139–2150.
38. Casjens S, van Vugt R, Tilly K, Rosa PA, Stevenson B (1997) Homology throughout the multiple 32-kilobase circular plasmids present in Lyme disease spirochetes. *J Bacteriol* 179(1):217–227.
39. Dunham-Ems SM, et al. (2009) Live imaging reveals a biphasic mode of dissemination of *Borrelia burgdorferi* within ticks. *J Clin Invest* 119(12):3652–3665.
40. Zückert WR (2007) Laboratory maintenance of *Borrelia burgdorferi*. *Curr Protoc Microbiol* Chap 12:Unit 12C.1.
41. Jutras BL, Chenail AM, Stevenson B (2013) Changes in bacterial growth rate govern expression of the *Borrelia burgdorferi* OspC and Erp infection-associated surface proteins. *J Bacteriol* 195(4):757–764.
42. Wagemakers A, Oei A, Fikrig MM, Miellet WR, Hovius JW (2014) The relapsing fever spirochete *Borrelia miyamotoi* is cultivable in a modified Kelly-Pettenkofer medium, and is resistant to human complement. *Parasit Vectors* 7:418.
43. Barocchi MA, et al. (2001) Identification of new repetitive element in *Leptospira interrogans* serovar copenhageni and its application to PCR-based differentiation of Leptospira serogroups. *J Clin Microbiol* 39(1):191–195.
44. Ellinghausen HC, Jr, McCullough WG (1965) Nutrition of *Leptospira pomona* and growth of 13 other serotypes: Fractionation of oleic albumin complex and a medium of bovine albumin and polysorbate 80. *Am J Vet Res* 26:45–51.
45. Fenno JC (2005) Laboratory maintenance of *Treponema denticola*. *Curr Protoc Microbiol* Chap 12:Unit 12B.1.
46. Kuru E, Tekkam S, Hall E, Brun YV, Van Nieuwenhze MS (2015) Synthesis of fluorescent D-amino acids and their use for probing peptidoglycan synthesis and bacterial growth *in situ*. *Nat Protoc* 10(1):33–52.
47. Glauner B (1988) Separation and quantification of muropeptides with high-performance liquid chromatography. *Anal Biochem* 172(2):451–464.
48. Bui NK, et al. (2009) The peptidoglycan sacculus of *Myxococcus xanthus* has unusual structural features and is degraded during glycerol-induced myxospore development. *J Bacteriol* 191(2):494–505.
49. Paintdakhi A, et al. (2016) Oufti: An integrated software package for high-accuracy, high-throughput quantitative microscopy analysis. *Mol Microbiol* 99(4):767–777.